Inorg. Chem. **2007**, *46*, 1283–1290

Copper(I)–Rhenate Hybrids: Syntheses, Structures, and Optical Properties

Haisheng Lin and Paul A. Maggard*

Department of Chemistry, North Carolina State University, Raleigh, North Carolina 27695-8204

Received September 18, 2006

The new copper(I) rhenates, $CuReO_4(pyz)$ (**I**) and $Cu_3ReO_4(q6c)_2$ (**II**) (pyz = pyrazine; q6c = quinoline-6-carboxylate), were synthesized by hydrothermal methods at 140–150 °C, and their structures determined via single-crystal X-ray diffraction (**I**, $P2_1/n$, No. 14, $Z = 4$, $a = 7.972(1)$ Å, $b = 11.928(2)$ Å, $c = 8.430(1)$ Å, $\beta = 102.161(2)°$; **II**, $P2_1$, No. 4, $Z = 2$, $a = 8.253(2)$ Å, $b = 6.841(2)$ Å, $c = 18.256(6)$ Å, $\beta = 101.37(2)°$) and characterized by thermogravimetric analyses and UV–vis diffuse reflectance. The structure of **I** contains '$CuReO_4$' layers that are pillared through bridging pyrazine ligands via the Cu sites, while the structure of **II** is polar and contains chains of 'Cu_2ReO_4' that are condensed into layers by coordination to linear '$Cu(q6c)_2$' bridges between the chains. In contrast to air-sensitive $CuReO_4$, both hybrid analogues are stable in air owing to a stabilization of the Cu^{1+} oxidation state by N-donating ligands, but decompose upon heating with the removal of the organic ligands, which for **I** yields crystalline $CuReO_4$. UV–vis diffuse reflectance measurements and electronic structure calculations on all three copper perrhenates, **I**, **II**, and $CuReO_4$, show that each exhibits an optical band gap of ~2.1–2.2 eV, with conduction and valence band levels that are primarily derived from the Re d^0 and Cu d^{10} orbitals, respectively, and mixed with O p-orbital contributions. In contrast to the silver rhenates, which have relatively lower energy Ag d^{10} orbitals, the inclusion of the organic ligands into the structures has only a very minor effect (~0.1 eV) on the band gap size. The optical absorptions, in combination with the air-stable open-framework layered structures, illustrate that heterometallic Cu^{1+}/Re^{7+} oxides can be promising candidates for investigating in visible-light photocatalytic reactions.

Introduction

Growing investigations into the chemical compatibility and structural synergy between metal-oxide and organic species during hydrothermal reactions have led to many new strategies for targeting highly functionalized metal-oxide/organic solids. For example, the selective coordination of an organic ligand, in combination with both an early and late transition metal, can be utilized to achieve new types of layered structures, such as in the multilayered $M(pyz)V_4O_{10}$ (M = Co, Ni, Zn)[1] (pyz = pyrazine) or in the pillared $M(pzc)_2(H_2O)_xAgReO_4$ (M = Cu, Ni, Co; pzc = pyrazinecarboxylate) series and related solids.[2−6] Another recently emerging area is the use of heterometallic solids in photocatalyst systems, wherein a solid-state compound absorbs light and uses it to catalytically drive reactions at its surfaces for the production of hydrogen and oxygen from water, for example.

Current metal-oxide photocatalysts, such as TiO_2 or $NaTaO_3$,[7,8] absorb only ultraviolet light, owing to their large band gaps. However, the incorporation of both an early and late transition metal can result in a decreased band gap size and the absorption of lower-energy visible light. Recent reported examples include Ag_3VO_4,[9] Ag_2MoO_4,[10] and Ag-

* To whom correspondence should be addressed. Phone: (+1) 919-515-3616. Fax: (+1) 919-515-5079. E-mail: Paul_Maggard@ncsu.edu.

(1) Yan, B.; Luo, J.; Dube, P.; Sefat, A. S.; Greedan, J. E.; Maggard, P. A. *Inorg. Chem.* **2006**, *45* (13), 5109.
(2) Yan, B.; Capracotta, M. D.; Maggard, P. A. *Inorg. Chem.* **2005**, *44* (19), 6509.
(3) Lin, H.; Yan, B.; Boyle, P. D.; Maggard, P. A. *J. Solid State Chem.* **2006**, *179* (1), 217.
(4) Maggard, P. A.; Yan, B.; Luo, J. *Angew. Chem., Int. Ed.* **2005**, *44* (17), 2553.
(5) Luo, J.; Alexander, B.; Wagner, T. R.; Maggard, P. A. *Inorg. Chem.* **2004**, *43* (18), 5537.
(6) Yan, B.; Maggard, P. A. *Inorg. Chem.* **2006**, *45* (12), 4721.
(7) Fujishima, A.; Honda, K. *Nature* **1972**, *238* (5358), 37.
(8) (a) Kato, H.; Asakura, K.; Kudo, A. *J. Am. Chem. Soc.* **2003**, *125* (10), 3082. (b) Porob, D. G.; Maggard, P. A. *J. Solid St. Chem.* **2006**, *179* (6), 1727.
(9) Konta, R.; Kato, H.; Kobayashi, H.; Kudo, A. *Phys. Chem. Chem. Phys.* **2003**, *5*, 3061.

10.1021/ic061767g CCC: $37.00
Published on Web 01/27/2007

TaO_3,[11] where each contains both a late (Ag^+) and early (V^{5+}, Mo^{6+}, Ta^{5+}) transition metal. These absorb visible light owing to an ~0.5 eV decrease of their band gap sizes, relative to the alkali metal versions, that arises from the Ag $4d^{10}$ orbitals mixing into and raising the valence band energies. As an initial step to expand this chemistry to more diverse metal-oxide/organic formats, we have recently reported on the syntheses and optical properties of $AgReO_4(pyz)$ and $Ag_3Mo_2O_4F_7(pyz)_3$, which exhibit decreased band gap sizes compared to the inorganic versions.[3] Further, these types of metal-oxide/organics can reversibly absorb water, e.g., $M(pzc)_2(H_2O)_xAgReO_4$ (M = Co, Ni),[4] and/or be thermally converted to the inorganic version, e.g., $AgReO_4$, by heating to remove the organic components.

However, despite the rising interest in heterometallics for visible-light band gap absorption, there are little to no previous investigations of heterometallic-oxide photocatalysts containing Cu^+ (d^{10}), even though the substitution of Cu^+ for Ag^+ should be expected (from ionization energies; 20.29 vs 21.48 eV, respectively) to shift their optical absorption even more strongly into the visible region. Typical solid-state synthetic approaches have provided a relatively limited number of compounds and structural diversity in which to investigate the properties of Cu^+/(early transition metal) oxide systems, including, for example, $CuNb_3O_8$ and $CuNbO_3$,[12,13] Cu_2WO_4,[14] and $CuReO_4$[15] within the respective Cu^+/Nb^{5+}, Cu^+/W^{6+}, Cu^+/Re^{7+} systems. Further, the $CuReO_4$ compound decomposes in air to $Cu^{II}(ReO_4)_2 \cdot 4H_2O$, Cu_2O, and Cu(s). Hydrothermal synthesis of metal-oxide/organic analogues of these solids has the potential to dramatically expand this area of chemistry, such as we have demonstrated for the $AgReO_4$-based solids, and can also enable new investigations into the effects of open metal sites and microporosity,[4] chirality,[2] and organic functionality on their optical properties and photocatalytic behavior. To date, we have reported on two previous copper−rhenate hybrids, $[Cu_2(pzc)_2(H_2O)_2ReO_4]$ and $[Cu(pzc)(H_2O)ReO_4] \cdot 2H_2O$,[16] both of which contain Cu^{2+}, as opposed to only Cu^+ ions, and their optical properties and electronic structures were not investigated.

Reported herein are the hydrothermal syntheses of two new Cu^+−rhenate hybrid structures, $CuReO_4(pyz)$ (**I**) and $Cu_3ReO_4(q6c)_2$ (**II**) (pyz = pyrazine; q6c = quinoline-6-carboxylate) and that contain pyrazine-pillared '$CuReO_4$' layers in **I** and chains of 'Cu_2ReO_4' that are connected into layers via '$Cu(q6c)_2$' bridges in **II**. The latter hybrid is analyzed with respect to several interesting structural features, including a polar symmetry group from alignment of the ReO_4 tetrahedra, and a triangular arrangement of three Cu^+ ions with a short Cu−Cu distance. The optical properties of the copper−rhenate hybrids are analyzed with respect to their calculated electronic structures and to the isoelectronic silver−rhenate hybrid systems in order to discern the origin of their smaller band gap sizes and to evaluate their potential in photocatalytic reaction systems.

Experimental Section

Materials. Cu_2O (99% metal basis, Alfa Aesar), Re_2O_7 (99.9+%, Alfa Aesar), pyrazine (99+%, Aldrich), and quinoline-6-carboxylic acid (98%, Alfa Aesar) were used as received. A reagent amount of deionized water was also used in each of the reactions, as well as used for the backfill into the hydrothermal reaction vessel.

Synthesis. $CuReO_4(pyz)$. The synthesis was performed by adding weighed amounts of pyrazine (35.2 mg, 0.44mmol), Cu_2O (31.5 mg, 0.22mmol), Re_2O_7 (106.6 mg, 0.22mmol), and H_2O (0.32 g, 17.6mmol), at a 1:1:1:40 (pyz/Cu/Re/H_2O) molar ratio, into a 3 in. × 4 in. FEP Teflon pouch that was subsequently heat sealed. Next, the pouch was placed inside a 125 mL Teflon-lined stainless-steel reaction vessel that was backfilled with ~40 mL of deionized water before closing. The reaction vessel was placed inside a convection oven and heated to 150 °C for 3 days, followed by slow cooling to room temperature at a rate of 6 °C h^{-1}. Faster cooling rates result in smaller and lower-quality crystals. After cooling, the products were immediately filtered and gave orange-colored brick-shaped crystals in high purity and in ~75% yield based on Cu.

$Cu_3ReO_4(q6c)_2$. Weighed amounts of quinoline-6-carboxylic acid (34.6 mg, 0.20mmol), Cu_2O (43.2 mg, 0.30mmol), Re_2O_7 (96.8 mg, 0.20mmol), and H_2O (0.27 g, 15mmol), in a 1:3:2:75 (q6c/Cu/Re/H_2O) molar ratio, were mixed and heat sealed inside a 3 in. × 4 in. FEP Teflon pouch. Next, the pouch was loaded into Teflon-lined stainless steel reaction, as before, and heated inside a convection oven to 140 °C for 24 h, and then slow cooled to room temperature at a rate of 6 °C h^{-1}. Brown block-shaped crystals were obtained as the primary product after filtering, with a few big gray-green tabular powders as a side product. The large brown crystals were easily manually separated and weighed to give a yield of ~36% based on Cu. The low yields likely result from the oxidation of Cu (green side products) and/or the decomposition of the organic ligand. The manually extracted crystals were also used in subsequent physical property measurements.

Structure Determination. An orange single crystal of dimensions 0.10 mm × 0.11 mm × 0.42 mm for **I** was selected for data collection on a Bruker-Nonius CCD diffractometer operating at a temperature of 193 K and using graphite-monochromatized Mo $K\alpha_1$ radiation ($\lambda = 0.71073$ Å). The unit cell parameters were determined with the Bruker SMART program using all observed reflections within a range of $7.92° < 2\theta < 60.92°$, which totaled 5984 reflections, of which 1699 were unique and observed ($F > 1\sigma_F$). The unit cell was determined to be monoclinic with $a = 7.972(1)$ Å, $b = 11.928(2)$ Å, $c = 8.430(1)$ Å, and $\beta = 102.161(2)°$. The data reduction was performed using the SAINT program,[17] and an absorption correction was applied using the SADABS program.[18] The structure was solved in the monoclinic space group $P2_1/n$ (No.

(10) Kato, H.; Matsudo, N.; Kudo, A. *Chem. Lett.* **2004**, *33*, 1216.
(11) Kato, H.; Kobayashi, H.; Kudo, A. *J. Phys. Chem. B* **2002**, *106*, 12441.
(12) Marinder, B. O.; Werner, P. E.; Wahlstroem, E.; Malmros, G. *Acta Chem. Scan. Ser. A* **1980**, *34*, 51.
(13) Marinder, B. O.; Wahlstroem, E. *Chem. Script.* **1984**, *23*, 157.
(14) Marinder, B. O.; Wang, P. L.; Werner, P. E.; Westdahl, M.; Andersen, A. F.; Louer, D. *Acta Chem. Scan. Ser. A* **1987**, *41*, 152.
(15) Mikhailova, D.; Ehrenberg, H.; Fuess, H. *J. Solid State Chem.* **2006**, *179*, 2004.
(16) Luo, J.; Alexander B.; Wagner, T. R.; Maggard, P. A. *Inorg. Chem.* **2004**, *43*, 5537.
(17) *SMART Ver. 5.625 Data Collection and SAINT-Plus ver. 6.22 Data processing for SMART System*; Bruker Analytical X-ray instruments, Inc.: Madison, WI, 2001.
(18) Sheldrick, G. M. *SADABS ver. 2.03, Software for Area Detector Absorptions and Other Corrections*; Bruker Analytical X-ray Instruments, Inc.: Madison, WI, 2001.

Table 1. Selected Single Crystal and Refinement Data for $CuReO_4(pyz)$ (**I**) and $Cu_3ReO_4(q6c)_2$ (**II**)

compound	**I**	**II**
fw (g/mol)	393.84	744.0
space group, Z	$P2_1/n$ (No.14), 4	$P2_1$ (No.4), 2
T (K)	193	293
a (Å)	7.972(1)	8.253(2)
b (Å)	11.928(2)	6.841(2)
c (Å)	8.430(1)	18.256(6)
β (deg)	102.161(2)	101.37(2)
V (Å^3)	783.55(39)	1010.4(5)
μ (Mo K$_\alpha$), mm^{-1}	18.12	9.140
d_{calcd}, (g cm^{-3})	3.34	2.581
reflns (total), R_{int}	5984	9465
data/restraints/params	1699/0/110	4614/1/308
final R1,wR2[a] [$I > 2\sigma(I)$]	0.056, 0.152	0.0301, 0.0798

[a] $R1 = \sum||F_o| - |F_c||/\sum|F_o|$; $wR2 = \{\sum[w(F_o^2 - F_c^2)^2]/\sum w(F_o^2)^2]\}^{1/2}$, $w = \sigma_F^{-2}$.

14) and refined using SHELXTL-97.[19] Hydrogen atoms on the pyrazine rings were refined in idealized positions at a C−H distance of 0.95 Å. The final anisotropic structure refinement converged at R1/wR2 = 0.056/0.152, with a data/variable ratio of ∼15:1. A secondary extinction coefficient was also included in the final cycles of refinement.

A brown single crystal of **II** was mounted for data collection on a Bruker SMART APEX CCD diffractometer as before. The unit cell parameters were determined using all observed reflections in the range of $4.56° < 2\theta < 57.68°$, which totaled 9465 reflections, of which 4614 were unique and observed ($F > 1\sigma_F$). The unit cell was determined to be monoclinic with $a = 8.253(2)$ Å, $b = 6.841(2)$ Å, $c = 18.256(6)$ Å, and $\beta = 101.37(2)°$. The structure was solved and refined using SHELXTL-97[19] in the monoclinic space group $P2_1$ (No. 4), and the resultant structure solution was checked for additional symmetry elements using the program PLATON.[20] Hydrogen atoms on the quinoline-6-carboxylic ligands were refined to ride on idealized positions around the carbon atoms in the ring. The Flack parameter refined to 0.633(8) and is indicative of racemic twinning which can occur in acentric single crystals.[21] The final anisotropic structure refinement converged at R1/wR2 = 0.0301/0.0798, at a data/variable ratio of ∼15:1.

Selected data collection and X-ray refinement parameters are listed in Table 1 for each of the respective structures of **I** and **II**. The atomic coordinates and isotropic-equivalent displacement parameters for each are give in Tables 2 and 3. The closest interatomic distances and bond angles are listed in Tables 4 and 5. The Supporting Information (CIF) contains a complete listing of data collection, refinement and anisotropic displacement parameters, and all nearest-neighbor interatomic distances and angles.

Thermogravimetric Analyses. Weighed samples of 24.86 mg of **I** and 5.08 mg of **II** were loaded onto Pt pans, equilibrated and tarred at room temperature, and heated at a rate of 5 °C min^{-1} for **I** and 1 °C min^{-1} for **II** to 400 °C under flowing nitrogen on a TA Instruments TGA Q50.

Optical Property Characterization. The UV−vis diffuse reflectance spectra were measured on a Cary 300 spectrophotometer equipped with an integrating sphere. Approximately 50 mg of powder of each sample was mounted onto a fused-silica holder and placed along the external window. A pressed polytetrafluoroethylene powder was used as a reference, and the data were plotted as the remission function $F(R_\infty) = (1 - R_\infty)^2/(2R_\infty)$, where R is diffuse reflectance based on the Kubelka−Monk theory of diffuse reflectance.

Table 2. Selected Atomic Coordinates and Equivalent Isotropic Displacement Parameters (Å^2) for $CuReO_4(pyz)$

atom[a]	x	y	z	U(eq)[b]
Re1	0.12820(4)	0.75334(2)	0.54188(3)	0.0204(3)
Cu1	−0.33309(9)	1.04084(7)	0.17448(8)	0.0255(3)
O1	0.282(1)	0.7465(3)	0.7207(6)	0.032(2)
O2	0.0120(7)	0.6274(5)	0.5146(7)	0.030(1)
O3	−0.0030(9)	0.8649(6)	0.5493(8)	0.045(2)
O4	0.230(1)	0.7721(6)	0.3818(9)	0.043(2)
N1	−0.4357(7)	1.0169(5)	0.3595(6)	0.020(1)
N2	−0.1360(7)	1.0233(4)	0.0752(6)	0.021(1)
C1	−0.3896(8)	0.9284(6)	0.4567(7)	0.023(1)
C2	−0.550(2)	1.089(3)	0.4026(6)	0.024(1)
C3	−0.1420(8)	1.0515(5)	−0.0797(8)	0.021(1)
C4	0.00749(9)	0.9703(6)	0.1547(8)	0.025(1)

[a] All atoms are located on a 4e Wyckoff site. [b] U(eq) is defined as one-third of the trace of the orthogonalized U_{ij} tensor.

Table 3. Selected Atomic Coordinates and Equivalent Isotropic Displacement Parameters (Å^2) for $Cu_3ReO_4(q6c)_2$

atom[a]	x	y	z	U(eq)[b]
Re1	0.23857(2)	0.70216(7)	−0.25376(1)	0.01712(7)
Cu1	0.60166(8)	0.47323(9)	−0.23109(4)	0.0212(2)
Cu2	−0.14727(8)	0.49539(10)	−0.29097(4)	0.0225(2)
Cu3	0.22325(9)	0.57755(13)	0.24094(3)	0.0234(2)
O1	0.4846(5)	0.4371(6)	0.6681(2)	0.0223(8)
O2	0.7009(5)	0.5090(6)	0.6154(2)	0.0229(8)
O3	0.3535(5)	0.5239(6)	−0.2008(2)	0.032(1)
O4	0.0829(5)	0.6025(6)	−0.3213(2)	0.029(1)
O5	0.9688(5)	0.4680(6)	−0.1895(2)	0.0239(9)
O6	0.7467(5)	0.5140(6)	−0.1380(2)	0.0238(8)
O7	0.3700(6)	0.8391(7)	−0.2963(3)	0.031(1)
O8	0.1551(6)	0.8544(8)	−0.1955(3)	0.026(1)
N1	0.1335(6)	0.5821(7)	0.3287(3)	0.0203(9)
N2	0.3137(6)	0.5630(7)	0.1533(3)	0.022(1)
C1	0.1657(7)	0.5593(8)	0.4636(3)	0.018(1)
C2	0.2721(7)	0.5285(8)	0.5341(3)	0.018(1)
C3	0.5023(7)	0.4821(8)	0.4727(3)	0.021(1)
C4	0.3995(7)	0.5037(8)	0.4032(3)	0.019(1)
C5	0.5505(7)	0.4766(8)	0.6136(3)	0.017(1)
C6	0.5497(8)	0.6020(1)	0.0953(4)	0.028(1)
C7	0.2143(7)	0.5415(7)	0.0832(3)	0.017(1)
C8	0.2837(7)	0.5467(7)	0.0176(3)	0.018(1)
C9	0.0426(7)	0.5173(8)	0.0763(3)	0.021(1)
C10	0.9021(7)	0.6432(9)	0.3879(3)	0.026(1)
C11	0.4748(8)	0.5919(9)	0.1576(3)	0.026(1)
C12	0.1784(7)	0.5264(8)	−0.0531(3)	0.018(1)
C13	0.0010(7)	0.5101(8)	−0.0583(3)	0.018(1)
C14	0.9428(7)	0.5042(8)	0.0067(3)	0.020(1)
C15	0.9747(7)	0.6318(9)	0.3255(3)	0.024(1)
C16	0.9956(8)	0.6074(9)	0.4578(3)	0.023(1)
C17	0.4367(7)	0.4943(7)	0.5376(3)	0.018(1)
C18	0.4573(8)	0.5779(9)	0.0254(3)	0.025(1)
C19	0.8999(7)	0.4954(8)	−0.1342(3)	0.018(1)
C20	0.2310(7)	0.5472(8)	0.3983(3)	0.018(1)

[a] All atoms are located on a 2a Wyckoff site. [b] U(eq) is defined as one-third of the trace of the orthogonalized U_{ij} tensor.

Electronic Band Structure Calculations. Extended Hückel electronic structure calculations were carried out within the tight-binding approximation using the CAESAR2 program,[22] using the full structures of **I** and **II** at 960 k-points spread over the irreducible wedge. The internal double-ζ basis sets were selected for the atomic orbital parameters, and the atomic coordinates and lattice dimen-

(19) Sheldrick, G. M. *SHELXTL NT ver. 6.10, Software Package for the Refinement of Crystal Structures*; Bruker Analytical X-ray Instruments, Inc.: Madison, WI, 2000.
(20) Spek, A. L. *PLATON*; Utecht University: Utecht, The Netherlands, 2001.
(21) Flack, H. D.; Bernardinelli, G. *J. Appl. Crystallogr.* **2000**, *33*, 1143.
(22) Whangbo, M.-H. *CAESAR2*; Department of Chemistry, North Carolina State University: Raleigh, NC, 1998.

Table 4. Selected Interatomic Distances (Å) in $CuReO_4(pyz)$ (**I**) and $Cu_3ReO_4(q6c)_2$ (**II**)

atom 1	atom 2	distance (Å)	atom 1	atom 2	distance (Å)
		I, $CuReO_4(pyz)$			
Cu1	N1	1.929(5)	Re1	O1	1.734(8)
	N2	1.940(5)		O2	1.754(6)
	O1	2.688(6)		O3	1.702(7)
	O2	2.164(6)		O4	1.729(7)
	O2	2.582(6)			
		II, $Cu_3ReO_4(q6c)_2$			
Cu1	Cu2	2.531(1)	Re1	O3	1.721(4)
	O1	1.919(4)		O4	1.735(4)
	O3	2.251(4)		O7	1.729(5)
	O6	1.897(4)		O8	1.726(4)
Cu2	O2	1.912(4)			
	O4	2.206(4)			
	O5	1.919(4)			
Cu3	N1	1.893(5)			
	N2	1.897(5)			

Table 5. Selected Interatomic Angles (deg) in $CuReO_4(pyz)$ (**I**) and $Cu_3ReO_4(q6c)_2$ (**II**)

atoms	angle (deg)	atoms	angle (deg)
	I, $CuReO_4(pyz)$		
N1−Cu1−N2	148.459(5)	O1−Re−O2	109.8(2)
O2−Cu1−N2	91.858(4)	O1−Re−O3	109.5(3)
O2−Cu1−N1	109.881(4)	O1−Re−O4	108.8(4)
		O2−Re−O3	111.3(4)
		O2−Re−O4	109.3(3)
		O3−Re−O4	108.7(4)
	II, $Cu_3ReO_4(q6c)_2$		
O1−Cu1−O3	86.9(2)	O3−Re−O4	111.7(2)
O1−Cu1−O6	177.2(2)	O3−Re−O7	108.1(2)
O3−Cu1−O6	101.6(2)	O3−Re−O8	108.9(2)
O2−Cu2−O4	101.8(2)	O4−Re−O7	109.6(2)
O2−Cu2−O5	169.1(2)	O4−Re−O8	110.2(2)
O4−Cu2−O5	89.1(2)	O7−Re−O8	108.2(3)
N1−Cu3−N2	177.9(2)		

sions were imported from their respective crystal structures. Molecular orbital pictures were calculated using local structural fragments and analyzed and plotted using the associated SAMOA program and subroutines.[23]

Results and Discussion

Structures. The structure of **I**, $CuReO_4(pyz)$, is comprised of '$CuReO_4$' layers that are cross-linked by pyrazine ligands and separated at a shortest interlayer distance of ~2.78 Å, shown in Figure 1. The '$CuReO_4$' sheets thereby stack into a three-dimensional pillared-layered structure via bonding of the pyrazine ligands to the Cu^+ ions in separate layers. Selected interatomic distances and angles are listed in Tables 4 and 5, and a structural view perpendicular to a single layer is drawn in Figure 2. Each Cu^+ is approximately five coordinate, shown in Figure 2, with two Cu−N (1.929(5) and 1.940(5) Å) and one short and two long Cu−O (2.164(6), 2.582(6), and 2.688(6) Å) bonds in a highly distorted trigonal-bipyramidal coordination geometry, e.g., CuN_2O_3. The axial sites are occupied by the oxygen groups from two different ReO_4 tetrahedra, while the equatorial positions are coordinated by one oxygen group from ReO_4 and two nitrogen groups from the pyrazine ligands located above and below the layer. Each ReO_4 tetrahedron serves as a bridge between two Cu^+ sites within the layer and dimerizes the Cu^+ polyhedra through a single shared edge to give local $Cu_2(pyz)_4(ReO_4)_4$ units. The Cu1···Cu1 dimer is at 3.6587(4) Å. The ReO_4 tetrahedron is relatively regular, with Re−O distances that span 1.702(7)−1.754(6) Å and O−Re−O bond angles of 108.7(4)−111.3(4)°, as known for previous structures containing the perrhenate anion.[2−4]

Heterometallic rhenates/organics often exhibit similar local structural fragments as compared with condensed (non-organic) rhenates, and which help reveal the recurring bonding patterns that assemble from solution. For example, $AgReO_4(pyz)$ is constructed from layers that share a strong structural similarity to layers in the condensed $AgReO_4$,[3] and which are also present in the $M(pzc)_2(H_2O)_xAgReO_4$ (M = Co, Ni, Cu) series.[2,4] By contrast, the isoelectronic '$CuReO_4$' layers in **I** are dissimilar to any local structural fragments of the recently reported and chiral $CuReO_4$.[15] The $CuReO_4$ solid

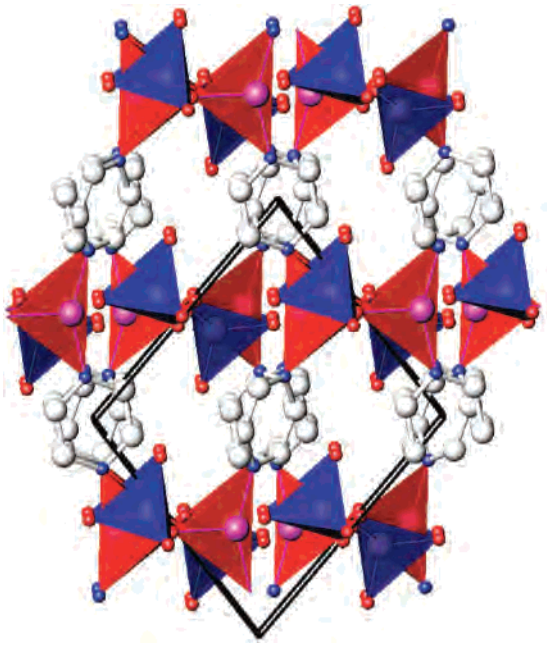

Figure 1. ~[010] polyhedral view of the $CuReO_4(pyrazine)$ structure with the unit cell outlined. Red polyhedra = Cu-centered coordination environments, blue polyhedra = ReO_4, red spheres = O, blue spheres = N, white spheres = C, purple spheres = Cu.

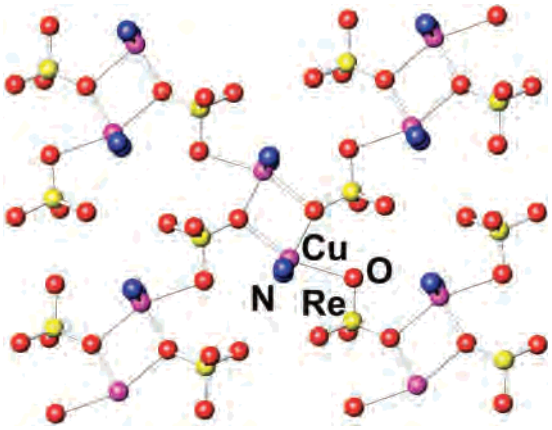

Figure 2. Structure of a single '$CuReO_4$' layer with selected atoms labeled. Red spheres = O, blue spheres = N, purple spheres = Cu, yellow spheres = Re.

(23) Whangbo, M.-H. *Structure and Molecular Orbital Analyzer* (*SAMOA*); North Carolina State University: Raleigh, NC, 2001.

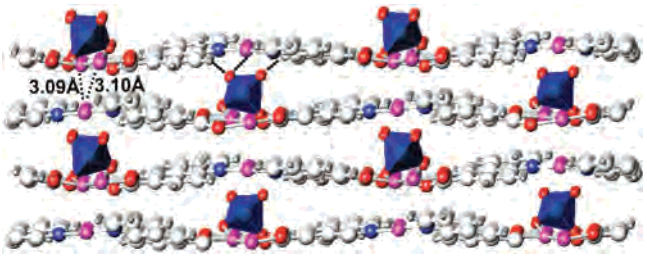

Figure 3. Structural view down the metal-oxide/organic layers of $Cu_3ReO_4(q6c)_2$. The dashed and solid lines mark the shortest Cu−Cu and C−H···O hydrogen bond distances between layers. Blue polyhedra = ReO_4, red ellipses = O, blue = N, white = C, and purple = Cu.

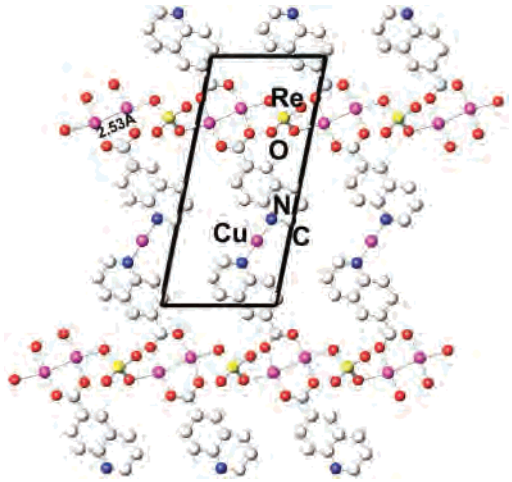

Figure 4. ~[010] structural view drawn perpendicular to a single layer of $Cu_3ReO_4(q6c)_2$. The shortest Cu−Cu distance and atom types are labeled.

is constructed from helical chains of tetrahedrally coordinated Cu and Re, e.g., MO_4, and that condense via corner-sharing into 4-, 6-, 8-, and 10-membered rings. In **I**, the local Cu environments are far from tetrahedral, as additional bonding interactions to the pyrazine ligands lead to a higher overall coordination number but a lower dimensionality of the oxide network. Also, edge-shared dimer motifs arise from a different bridging mode of the ReO_4 groups. These structural differences likely suppress the interconversion of the two solids at low temperatures (see below) but which is possible between $AgReO_4$ and $AgReO_4(pyz)$.

The dark-brown crystals of **II**, $Cu_3ReO_4(q6c)_2$, exhibit a unique layer structure comprised of undulating $[Cu_3ReO_4(q6c)_2]_\infty$ layers that stack with an offset of $1/2(a + c)$, shown in Figure 3. The shortest interlayer bonding interactions are the C−H···O hydrogen bonds and the Cu−Cu near neighbors, labeled with solid and dashed lines in Figure 3. Selected interatomic distances and angles are given in Tables 4 and 5, respectively. The bonding arrangement within an individual $[Cu_3ReO_4(q6c)_2]_\infty$ layer, shown in Figure 4, includes chains of 'Cu_2ReO_4' that are interconnected into layers via the bridging carboxylate groups of '$Cu(q6c)_2$' units. Thus, there are two types of Cu coordination environments. One type occurs in the 'Cu_2ReO_4' chains (Cu1 and Cu2) as Cu−Cu dimers that are edge-bridged by two carboxylate groups at Cu−O distances of 1.893(5)−1.919(4) Å, and coordinated by two ReO_4 groups at Cu−O distances of 2.206(4) and 2.251(4) Å. The dimer also exhibits a very short Cu−Cu distance of 2.531(1) Å, an interesting feature that has been found previously in other similar Cu^+-Cu^+ carboxylate-bridged dimers.[24−26] The existence of Cu^+-Cu^+ ($d^{10}-d^{10}$) bonding interactions, or 'cuprophilicity', for distances as short as ~2.45 Å in $Cu_2(hpp)_2$[24a] is highy controversial despite investigations into several known cases. The second type of Cu coordination environment, Cu3, occurs in the bridging '$Cu(q6c)_2$' units, where Cu is coordinated in a nearly linear fashion by two nitrogen groups from the two quinoline-6-carboxylate ligands at Cu−N distances of 1.893(5) Å and 1.897(5) Å with a N1−Cu3−N2 angle of 177.9(2)°. The next closest neighbors to Cu3 are at a much farther distance and are in the adjacent layer to the dimerized Cu atoms at ~3.09−3.10 Å and to ligand oxide groups at >3.15 Å.

Shown in Figure 3, the tetrahedral ReO_4 groups are aligned in a polar fashion down the *b* axis on one side of the $[Cu_3ReO_4(q6c)_2]_\infty$ layers and have nearly regular geometries with Re−O distances of 1.721(4)−1.735(4) Å and O−Re−O angles of 108.1−111.7°. Two of the O vertices are bonded to Cu1 and Cu2 within the 'Cu_2ReO_4' chains, while the other two O vertices form C−H···O hydrogen bonds to the carboxylate groups of the ligands in the adjacent layer. The C···O and H···O distances in the hydrogen bonds ($d_{C\cdots O}$=3.169, 3.188 Å; $d_{H\cdots O}$ = 2.315, 2.351 Å) are slightly shorter than the average distances (3.540, 2.553 Å) of reported C−H···O hydrogen bonds.[27]

Thermal Properties. The thermal stability and the removal of organic ligands from **I** and **II** was investigated by heating each sample under flowing N_2. It is notable that both solids are stable in air, while the 'organic-free' $CuReO_4$ is unstable in air and slowly decomposes to $Cu^{II}(ReO_4)_2{\cdot}4H_2O$, Cu_2O, and Cu(s).[15] The equilibrium governing the relative stability of Cu^+/Cu^{2+} oxidation states is known to depend on the types of ligands involved, with softer ligands (more covalent; CN^-, I^-) stabilizing Cu^+ and harder ligands (more ionic; ClO_4^-) showing a greater affinity for Cu^{2+}.[28] Thus, the additional covalent bonding provided by the softer N-donating ligands helps to more stongly stabilize the Cu^+ oxidation state and keeps the hybrid compounds from decomposing in air. Thermogravimetric analysis (TGA), plotted in Figure 5, indicates that upon heating the organic ligands are removed/decomposed beginning at temperatures of ~190 °C for **I** and ~290 °C for **II**. The higher decomposition temperature of **II** likely owes to the presence of more strongly bonded carboxylate groups, see for example $AgReO_4(pyz)$ vs $M(pzc)_2(H_2O)_2AgReO_4$.[3,4] The TGA of **I** also exhibits two weight-loss steps, one of 9.4% between 190 and 275 °C, and another of 9.6% between 275 and 400 °C. The total weight loss of 19% matches well with that expected from the removal of all pyrazine ligands

(24) a) Cotton, F. A.; Feng, X.; Timmons, D. J. *Inorg. Chem.* **1998**, *37*, 4066; b) Clérac, R.; Cotton, F. A.; Daniels, L. M.; Gu, J.; Murillo, C. A.; Zhou, H.-C. *Inorg. Chem.* **2000**, *39*, 4488.
(25) Che, C. M.; Mao, Z.; Miskowski, V. M.; Tse, M. C.; Chan, C. K.; Cheung, K. K.; Phillips, D. L.; Leung, K. H. *Angew. Chem., Int. Ed.* **2000**, *39*, 4084.
(26) Mehrotra, P. K.; Hoffmann, R. *Inorg. Chem.* **1978**, *17*, 2187.
(27) Steiner, T. *Angew. Chem., Int. Ed.* **2002**, *41*, 48.
(28) Cotton, F. A.; Wilkinson, G. *Advanced Inorganic Chemistry*, 5th ed.; John Wiley and Sons: New York, 1988; p 755.

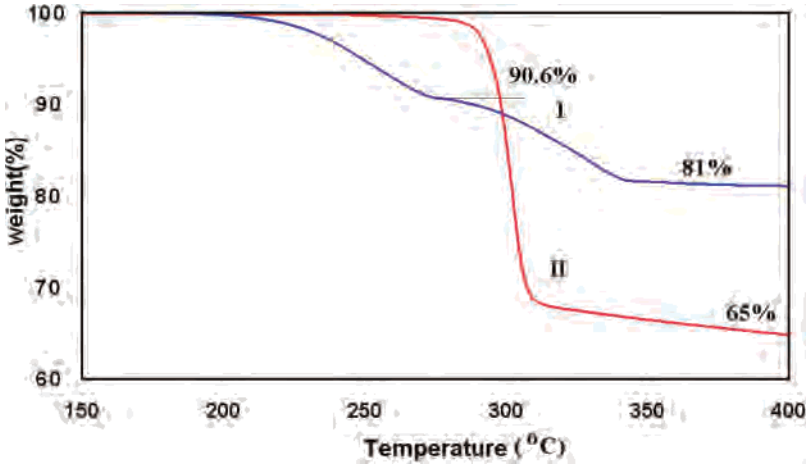

Figure 5. Thermogravimetric analysis of **I** and **II**, plotted as weight % versus temperature (°C).

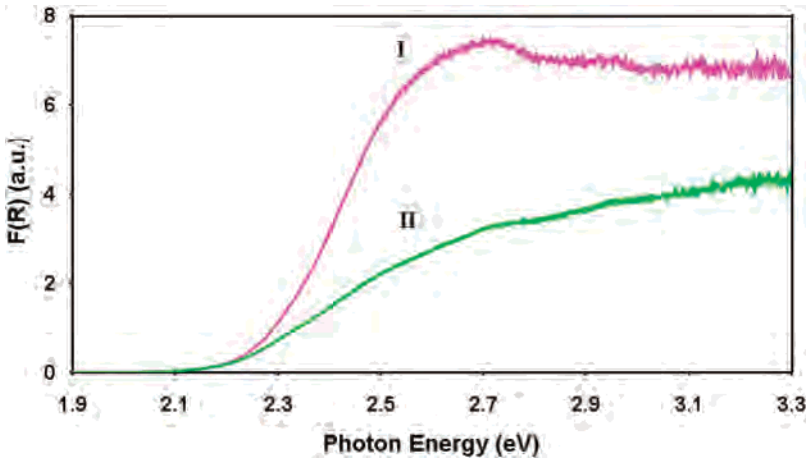

Figure 6. UV−vis diffuse reflectance spectra of **I** and **II**, plotted as a function of the photon energy in eV.

(theoretical weight loss = 20%). The powder X-ray diffraction (PXRD) of the orange-colored residue from the first weight-loss step (Supporting Information) indicates an unidentified crystalline structure. The PXRD data of the final brown residue after the second weight loss was confirmed to be $CuReO_4$ (Supporting Information), with some additional small diffraction peaks owing to $Cu^{II}(ReO_4)_2$ because of exposure of the product to air for a short time. The TGA of **II** revealed a single weight loss step of ~35% by 400 °C, indicating only an incomplete removal of the ligands (theoretical weight loss = 44%), and which continues slowly at higher temperatures. The final residue was an amorphous black material that was not characterized further.

Optical Properties and Electronic Structure Calculations. Heterometallic oxides that contain both a late (Ag^+) and early (V^{5+}, Mo^{6+}, Ta^{5+}) transition metal, with d^{10} and d^0 electron configurations respectively, have been investigated for their absorption of visible light ($E_g \approx 2.2-3.0$ eV) and ability to drive photocatalytic reactions.[9−11] In order to analyze the influence of Cu^+ on the optical absorption energies, the UV−vis diffuse reflectance spectra of **I** and **II** were measured, shown in Figure 6. Both exhibited a strong optical absorption in the visible region, with optical band gaps of ~2.23 and ~2.20 eV for **I** and **II**, respectively, as calculated from the onset of their absorption edges. These band gap sizes are significantly smaller than in $AgReO_4$ (3.7 eV) or $AgReO_4$(pyz) (2.9 eV),[3] arising from the replacement of lower-energy d orbitals of Ag^+ for the higher-energy d orbitals of Cu^+. Thus, a much larger fraction of visible-light is absorbed by these Cu^+-containing heterometallic oxides.

The electronic structures of **I** and **II** were calculated on the basis of the Extended Hückel approach, both in order to evaluate the atomic-orbital contributions to the valence and conduction bands and to analyze the factors that influence the sizes of their optical band gaps. Contour maps of the electron density of the calculated HOMO and LUMO for local structure fragments of **I**, **II**, and $CuReO_4$ are shown in Figure 7. Also, shown in Figure 8 are the total densities-of-states (DOS) overlaid with the projected partial densities-of-states (PDOS) for each element. In all three structures, the lowest unoccupied orbitals in the conduction band were confirmed to derive from the Re 5d and O 2p orbitals, as seen in the PDOS in Figure 8 and in the local orbital pictures in Figure 7. The highest occupied orbitals of all three are fairly similar and are formed mainly from the Cu 3d, N 2p, and O 2p orbitals. However, the band gap of **II** is calculated to be slightly smaller than that of **I** and contains no contributions from the N 2p orbitals in its highest-energy

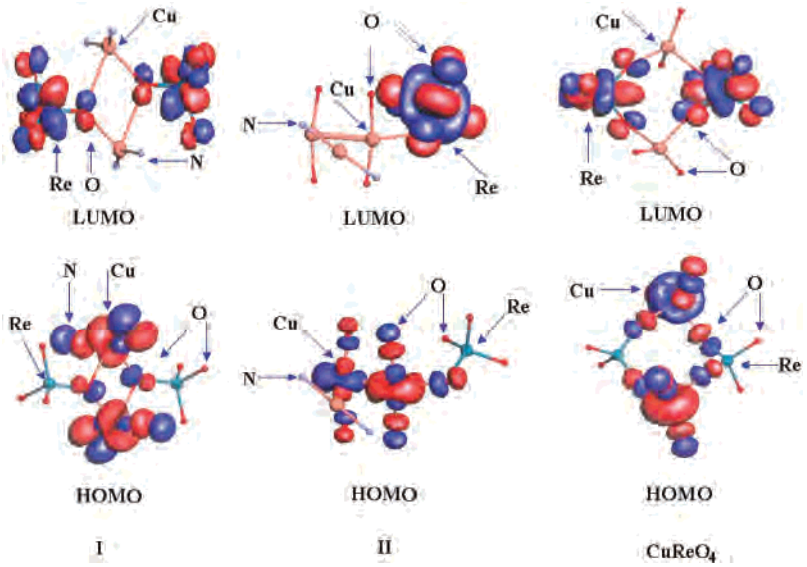

Figure 7. Electron density contour maps of the calculated LUMO and HOMO of local structural fragments in $CuReO_4(pyz)$ (**I**), $Cu_3ReO_4(q6c)_2$ (**II**), and $CuReO_4$.

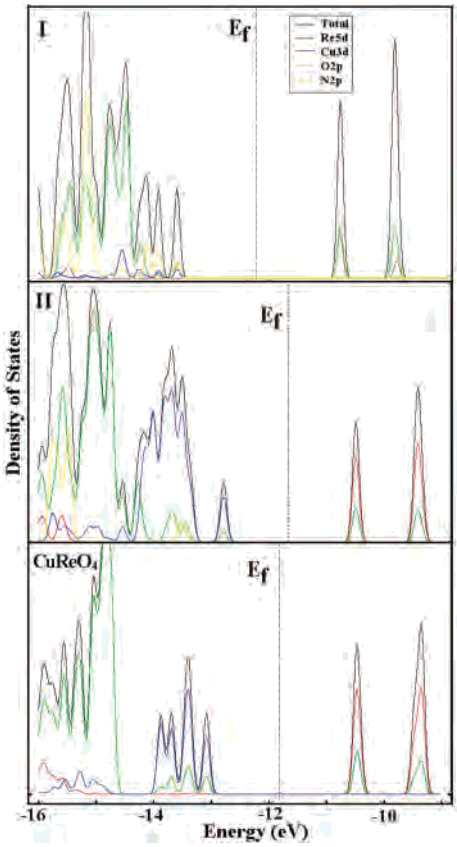

Figure 8. Calculated total and projected densities-of-states for $CuReO_4(pyz)$ (**I**), $Cu_3ReO_4(q6c)_2$ (**II**), and $CuReO_4$.

valence band levels. Therefore, the optical excitation from the valence to the conduction band can be viewed as a metal-to-metal charge transfer between Cu^+ (d^{10}) and Re^{7+} (d^0), with moderate contributions from the ligand-based orbitals.

As the measured optical band gaps for **I** and **II** are a relatively constant ~2.2 eV, the contribution and effect of the overall structures and organic ligands to the relevant valence and conduction band levels appear minimal (≤0.1 eV). Diffuse reflectance spectra taken on the TGA residuals after removal of 50% of the pyrazine ligands in **I**, i.e., $CuReO_4(pyz)_{0.5}$, and after the complete removal of the ligand to give crystalline $CuReO_4$, gave optical band gaps of 2.20 and 2.10 eV, respectively (Supporting Information). This trend confirms the band gap size is effected only slightly by the removal of pyrazine, causing it to decrease slightly. By comparison, the loss of pyrazine ligands from $AgReO_4(pyz)$ to give $AgReO_4$ causes a dramatic increase in the band gap from 2.91 to 3.71 eV.[7] This arises because the pyrazine orbitals mix into the valence bands at energies higher than the Ag $4d^{10}$ electrons. For $CuReO_4(pyz)$, however, the pyrazine orbitals are lower in energy than the Cu 3d orbitals which comprise the valence band, and therefore the ligand orbitals have a smaller effect on the magnitude of the band gap size.

The positions of the conduction and valence bands, with respect to relevant redox couples, are also of significant importance in photocatalytic reactions. Band gap trends in these and related heterometallic oxides suggest that Re and Cu d orbitals straddle the redox potentials for the oxidation and reduction of water, and will be reported in a separate paper on this topic. Initial photocatalysis testing of these solids, however, including the oxidation of methanol or the reduction of Ag^+ over their surfaces, does not show any detectable activity. Kinetic factors likely begin to play a more dominant role for smaller band gap sizes and thus requires a closer analysis of the local coordination sites, as well as the potential mechanisms of electron transfer. However, the optical properties and electronic structures of these solids illustrate the high potential for Cu^+-containing heterometallics for the discovery of active photocatalysts with smaller visible-light band gaps.

Conclusions

New copper(I) rhenate hybrids, $CuReO_4(pyz)$ (**I**) and $Cu_3ReO_4(q6c)_2$ (**II**), have been synthesized hydrothermally and feature '$CuReO_4$' layers and 'Cu_2ReO_4' chains, respectively, and that are bridged by pyrazine and '$Cu(q6c)_2$' units into

3D and 2D structures. The structure of **II** has a polar symmetry group from the alignment of ReO_4 between the layers and also contains a short Cu−Cu distance from bonding to the bridging carboxylate groups on the ligands. Both hybrids are stable in air but decompose upon heating with the removal of the organic ligands, which for **I** yields crystalline $CuReO_4$. Both exhibit relatively low-energy optical band gaps of ∼2.2 eV, compared to ∼2.9 eV for that of $AgReO_4$(pyz), that arise from the higher-energy d orbitals of Cu^+ compared to Ag^+. Electronic structure calculations confirm the valence and conduction bands derive primarily from the Cu d^{10} and Re d^0 orbitals, respectively. Further synthetic studies are in progress in the heterometallic Cu^+/Re^{7+} system in order to better probe the effects of local structure on the optical band gaps and potential photocatalysis mechanisms.

Acknowledgment. P.M. acknowledges support from the Beckman Foundation as a Beckman Young Investigator and from the American Chemical Society Petroleum Research Fund (40963-G10).

Supporting Information Available: Crystallographic data in CIF format, and the PXRD and UV−vis diffuse reflectance of the TGA residues of **I**. This material is available free of charge via the Internet at http://pubs.acs.org.

IC061767G